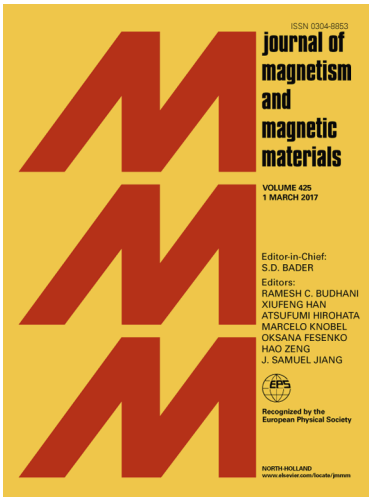

Structure and size dependence of the magnetic properties of Ni@C nanocomposites

A. Manukyan, A. Elsukova, A. Mirzakhanyan, H. Gyulasaryan, A. Kocharian, S. Sulyanov, M. Spasova, F. Römer, M. Farle, E. Sharoyan

PII: S0304-8853(18)30116-1
DOI: https://doi.org/10.1016/j.jmmm.2018.07.056
Reference: MAGMA 64162

To appear in: *Journal of Magnetism and Magnetic Materials*

Please cite this article as: A. Manukyan, A. Elsukova, A. Mirzakhanyan, H. Gyulasaryan, A. Kocharian, S. Sulyanov, M. Spasova, F. Römer, M. Farle, E. Sharoyan, Structure and size dependence of the magnetic properties of Ni@C nanocomposites, *Journal of Magnetism and Magnetic Materials* (2018), doi: https://doi.org/10.1016/j.jmmm.2018.07.056

Structure and size dependence of the magnetic properties of Ni@C nanocomposites

A. Manukyan[a,*], A. Elsukova[b], A. Mirzakhanyan[a], H. Gyulasaryan[a], A. Kocharian[c], S. Sulyanov[d], M. Spasova[b], F. Römer[b], M. Farle[b], E. Sharoyan[a]

[a] *Institute for Physical Research, National Academy of Sciences, Ashtarak 0203, Armenia*
[b] *Fakultät Physik and Center of Nanointegration Duisburg-Essen (CENiDE)*
[c] *California State University, Los Angeles, CA, 90032, USA*
[d] *National Research Center Kurchatov Institute, Moscow 123182, Russia*

Abstract

Carbon-coated nickel (Ni) nanoparticles, Ni@C nanocomposites, have been synthesized using solid-state pyrolysis of nickel phthalocyanine and metal-free phthalocyanine $(NiPc)_x{\cdot}(H_2Pc)_{1-x}$ solid solutions, $0 \le x \le 1$. The Ni concentrations in carbon matrix (c_{Ni}) of the prepared samples continuously varied in the range of 0–3at.% (0–12wt.%). The average nanoparticle size varied within 4-40 nm range. All samples containing single domain Ni nanoparticles exhibit both ferromagnetic and superparamagnetic properties because of the wide range of size distribution. An abrupt drop of saturation magnetization has been observed with decrease in size of Ni nanoparticles from 40 nm to 12 nm. Nearly linear dependence of saturation magnetization on the nanoparticle surface/volume ratio can be interpreted as a result of contact interaction between Ni nanoparticles and the carbon matrix which provides an electron transfer from carbon matrix to nickel. However, further reductions in nanoparticle size increase magnetization growth of which can apparently contribute to the emergence of the giant paramagnetism due to large orbital moments of conductive electrons. The size effects and surface magnetic anisotropy in Ni@C nanocomposites are revealed in the measurements of coercive field, zero-field cooling (ZFC) susceptibility, blocking temperatures and ferromagnetic resonance spectra. Concentration dependencies of ferromagnetic and electron paramagnetic resonance parameters in Ni@C nanocomposites have also been investigated and their peculiarities highlighted. A correlation between concentration dependencies of FMR and SQUID magnetometry parameters, namely between the g-factor curves - g_{eff}, the resonance linewidth - ΔH_{FMR} and coercive field - H_c, have been observed.

Keywords: Ni@C nanocomposites, magnetic properties, size sffect, SQUID magnetometry, FMR, EPR, solid-phase pyrolysis, solidsulutions of phthalocyanines.

1. Introduction

In recent years, magnetic nanoparticles have become a topic of great interest from the scientific point of view, since their potential applications have become increasingly apparent. In particular, these nanomaterials are used in biomedicine, spintronics, catalysis, sensors, supercapacitors, etc [1–9]. Applications of magnetic metallic nanoparticles (M) encapsulated in a carbon (graphitic) shell (M@C), as carbon matrices exhibit high chemical and thermal stability. The carbon shell not only protects metal nanoparticles from oxidation, but also prevents their aggregation. In addition, carbon is a biocompatible material.

Currently, there are several methods for preparation of metal nanoparticles, including hydrothermal, arc discharge, laser ablation, chemical vapour deposition, pyrolysis, reduction of metal salts, solvothermal and aquollic methods, etc [1–3, 10–13].

We have developed highly facile, simple, safe and cost-effective one-step method which is based on solid-state pyrolysis of organic and metal-organic compounds. In Refs. [14–16] we presented a method of solid-state pyrolysis in metal phthalocyanines – MPc [$M(C_{32}N_8H_{16})$, M= Ni, Cu, Fe, Co, Zn] powders. Using this method, we obtained metallic nanoparticles in various carbon matrices. In this case, the atomic concentration of nickel metal is 3 at.%. We also discovered that solid-state pyrolysis of metal-free phthalocyanine – H_2Pc [$H_2(C_{32}N_8H_{16})$] yields carbon microspheres, consisting of nanographite crystallites and amorphous carbon [17–19]. Diluting metal phthalocyanines with metal-free phthalocyanine and varying the solid-state pyrolysis parameters provides a unique opportunity to get insight into the dependences of structural and magnetic properties of nanoparticles on their size and concentration. One of the objectives of this work was preparation of metal phthalocyanine – metal-free phthalocyanine $(MPc)_x(H_2Pc)_{1-x}$, $0 \le x \le 1$ solid solutions. Pyrolysis of these solid solutions allows obtaining metallic nanoparticles in a range of concentration from 0 to 3 at.% (from 0 to 12 wt%).

In the present work we have syntesized nanocomposites in which the average size of Ni nanoparticles varies in a range from 4 nm to 40 nm. This was achieved by solid-phase pyrolysis of solid solutions $(NiPc)_x(H_2Pc)_{1-x}$, by changing composition - x and parameters of pyrolysis (temperature, time and pressure).

*Corresponding author
Email address: manukyan.ipr@gmail.com (A. Manukyan)

Ni nanoparticles encapsulated in a carbon matrix, Ni@C nanocomposites, were investigated in Refs. [20–28]. Depending on used synthetic techniques, Ni@C nanocomposites can have different carbon structures, morphology and magnetic characteristics. Despite a considerable number of works, no systematic research has been done on magnetic properties of Ni nanoparticles within a wide size range, including also ultra small, 1–10 nanometer scale. In this fine nanometric scale, physical properties of nanoparticles can strongly differ from that of bulk. Two important effects which define the characteristics of nanoparticles are the surface effect and the size effect. A particle size decrease leads to an increase in number of surface atoms with different structural topology. The interaction of surface atoms with a matrix is also very important and it can strongly change their valence state. In addition, when the particle size is sufficiently small, the Fermi wavelength of the electrons becomes comparable to the system linear size (d), and elastic length (l_e) of a free path of electrons in the ballistic regime can exceed its linear size: $l_e > d$ [29, 30].

Almost all prior works dedicated to the investigation of Ni@C nanocomposites [24–27] point at the lower values of saturation magnetization comparing to that of bulk Ni. The possible reasons of magnetization reduction with decrease in nanoparticle size are discussed in Refs. [27, 31–36]. In current work a drop of saturation magnetization in Ni@C nanocomposites has been described. It has been interpreted as a result of nanoparticles size decrease from 40 nm to 12 nm at 10K and hence increase in interaction surface between Ni nanoparticles and carbon shells. However, with further decline in Ni particle size from 12 nm to 4 nm no subsequent magnetization drop has been detected. On the contrary a noticeable increase of magnetization within that interval has been observed. It is obvious that small size 1-10 nm metal nanoparticles behave as quantum dots, i.e., quasi-atoms in which the significant changes of the electronic energy levels occur. The increase in magnetization apparently is driven by large orbital paramagnetism of conducting electrons in the ballistic regime.

Surface effects in 1-10 nm interval lead to a strengthening of the magnetic anisotropy effective constant K_{eff}. We have found the dependence of K_{eff} from size of Ni nanoparticles by measurements of ZFC susceptibility. As observed in our experiments, the increase in K_{eff} in fine nanoparticles enhances the coercive field as well as the blocking temperature. The fine nanoparticles with blocking temperatures at ≅ 43°C can have important practical applications in magnetic hyperthermia treatment of cancer disease. Fine nanoparticles with blocking temperatures higher than room temperature can also be used for high-density magnetic recording storage.

2. Synthesis of samples and investigation methods.

In earlier studies we have developed solid-phase pyrolysis of NiPc [$Ni(C_{32}N_8H_{16})$] powders and prepared Ni nanoparticles in different carbon matrices with 3 at.% (12 wt.%) atomic concentration of Ni [14, 15]. We have found that during solid-phase pyrolysis of H_2Pc [$H_2(C_{32}N_8H_{16})$] the formed carbon microspheres consist of graphite nanocrystallites and amorphous carbon [17–19].

In current work, the solid solutions of NiPc-H_2Pc have been prepared: $(NiPc)_x(H_2Pc)_{1-x}$, where $0 \le x \le 1$. Solid-phase pyrolysis of these solid solutions can be described by the following chemical reaction.

$$[Ni\,(C_{32}N_8H_{16})]_x\,[H_2\,(C_{32}N_8H_{16})]_{1-x} \xrightarrow[-8H_2,-4N_2]{T_{pyr},t_{pyr},p} Ni_x + 32C,\ 0 \le x \le 1 \quad (1)$$

where T_{pyr} is the pyrolysis temperature, t_{pyr} is the pyrolysis time and p is the pressure in a reaction ampoule. The pyrolysis conditions for all samples, except for $S_{2.5}$, were the same: T_{pyr} = 700 °C, t_{pyr} = 30 min. With the aim to synthesize Ni nanoparticles with small sizes and high Ni concentration, c_{Ni}, the pyrolysis time of the sample $S_{2.5}$ was significantly less.

It is easy to obtain the relation, which connects the Ni concentration (c_{Ni}) in the prepared compounds expressed in atomic percent with the values of x, used in reaction (1):

$$c_{Ni} = \frac{x}{32 + x} \cdot 100 at.\% \quad (2)$$

We have synthesized a large set of samples with the Ni concentration equal to 0, 0.5, 0.75, 1, 1.5, 2, 2.5 and 3 at.%. The average value of the Ni concentration taken in different parts of the sample $< c_{Ni} >$ coincides with the calculated values obtained by the formula (2) with the accuracy of 10%. The atomic concentration of Ni in our samples is noted as an subindex, i.e., samples S_0, $S_{0.5}$, $S_{0.75}$, S_1, $S_{1.5}$, S_2, $S_{2.5}$, and S_3 correspond to samples where the Ni concentrations are 0, 0.5, 0.75, 1, 1.5, 2, 2.5 and 3 at.%. The weight percents of Ni atoms in samples are respectively equal to 0, 2, 3, 4, 6, 8, 10 and 12 wt%.

The composition, structure, morphology, and particle size of fabricated composites have been investigated using scanning electron microscopes (SEM) LEO 1530 SEM operated at 30 kV with a field emission gun, high resolution transmission and scanning transmission electron microscopy (HRTEM and STEM) FEI Tecnai F20 Supertwin microscope operated at 200 kV with a field emission gun, and X-ray diffraction (XRD) spectrometer X′PERT PRO (PANalytical, Nederland′s) with the CuK_α radiation (λ = 1.5418 Å). Magnetic properties of Ni nanoparticles have been studied with an X-band (9.3 GHz) electron spin resonance spectrometer Bruker Elexsys II E 500, and a Quantum Design MPMS XL SQUID magnetometer.

3. Results and discussions

3.1. Structural investigations

3.1.1. X-ray diffractometry and Raman spectroscopy

Fig.1 presents X-ray diffraction spectra (XDS) of samples S_0-S_3 recorded at room temperature, where one can see the peaks from Ni and carbon. A broad peak at about 26° corresponds to graphite-like carbon structures and four narrow peaks with 2θ = 44.32° (111), 51.64° (200), 76.02° 220) and 92.44° (311) corresponds to Ni nanoparticles with a fcc structure. As can be also seen in this figure, the degree of graphitization of carbon strongly increases with increase in Ni concentration.

Table 1: Structural and magnetic characteristics of Ni@C nanocomposites at different Ni concentrations.

Sample	m wt.%	$< d > nm$	γ	$M_S\ (Ni@C, 10K)\ emu/g_{Ni}$	$M_S\ (Ni@C)\ /M_S\ (Ni_{bulk})$	M_R/M_S^{FM}		$< T_b >$°C
					10K	10K	300K	
$S_{0.5}$	2	4(2)	0.13	$6.1_{H=45kOe}$	$0.11_{H=45kOe}$	-	-	350
$S_{0.75}$	3	6(3)	0.33	$5_{H=45kOe}$	$0.09_{H=45kOe}$	0.44	0.31	190
S_1	4	17(5)	0.6	12	0.21	0.43	0.17	110
$S_{1.5}$	6	20(6)	0.6	12.2	0.22	0.50	0.15	200
S_2	8	23(13)	0.6	14.5	0.27	0.54	0.21	260
$S_{2.5}$	10	12(7)	0.8	4.9	0.09	0.57	0.17	330
S_3	12	26(14)	0.6	19	0.35	0.48	0.17	190
$^*S_3$	12	40(16)	0.9	29	0.50	0.51	0.25	-

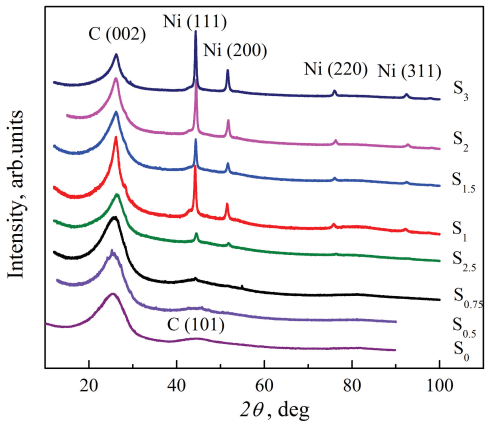

Figure 1: Room-temperature XRD patterns from samples of series S_0 to S_3 indicating the peaks of Ni and C.

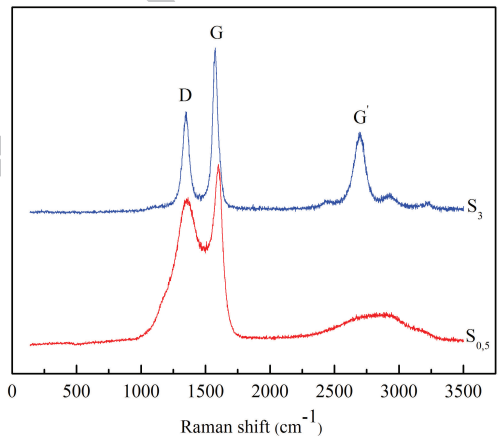

Figure 2: Raman spectra of the $S_{0.5}$ and S_3 samples.

The graphitization degree of carbon is calculated by the formula $\gamma = (3.50\text{-}d_{002})\ /(3.50\text{-}3.35)$, where d_{002} is interplanar distance between graphene layers measured from X-ray diffraction patterns. The γ values for S_0-S_3 are given in Table 1. For the sample S_0 the value is γ=0, which corresponds to the turbostratic phase of graphite with d_{002}=3.50 Å.

For investigation of the fine structure parameters (dispersity and microdeformations) we used the Williamson-Hall (W-H) method. It was difficult to determine a mean size of coherent scattering blocks. Broadening of X-ray diffraction lines is mainly determined not by dispersity, but rather by microdeformations. We calculated the slope tangents of Williamson-Hall plots, which characterized a mean value of microdeformations. Microdeformations increase with a decrease in the size of Ni nanoparticles. Shifts in Raman spectra for samples S_3 and $S_{0.5}$ are shown in Fig. 2. The bands D and G correspond to A_{1g} "defect" and E_{2g} "graphite" vibrations. D and G bands narrowing is observed under increase in the Ni concentration, which shows the increase in the graphitization degree. This is confirmed also by the sharp narrowing and increase in the second harmonic of the D band at 2693 nm. There is also a considerable shift of the G band in the $S_{0.5}$ sample (1601 cm^{-1}) compared to the S_3 sample (1574 cm^{-1}) that corresponds to transition from nanographite to more graphitized carbon structure. There are no peaks in the low-frequency interval (300-600 cm^{-1}) corresponding to nickel oxide, since carbon shell completely preserves nickel nanoparticles from oxidation.

3.1.2. SEM, STEM and TEM microscopes. Morphology. Size of nickel nanoparticles and their distribution.

In solid-phase pyrolysis of metal-free phtalocyanine, when c_{Ni}=0, formation of carbon microspheres with mean size of ≈ 3.5(1) μm takes place [17]. Morphology of samples prepared by solid-phase pyrolysis of solid solutions $(NiPc)_x(H_2Pc)_{1\text{-}x}$ strongly depends on x and pyrolysis conditions (temperature, time and pressure). We have prepared Ni nanoparticles encapsulated in graphite-like coatings Ni@C. In general they can be embedded in carbon plates, carbon microspheres, carbon fibers and nanotubes either separately or as a mixture of different mor-

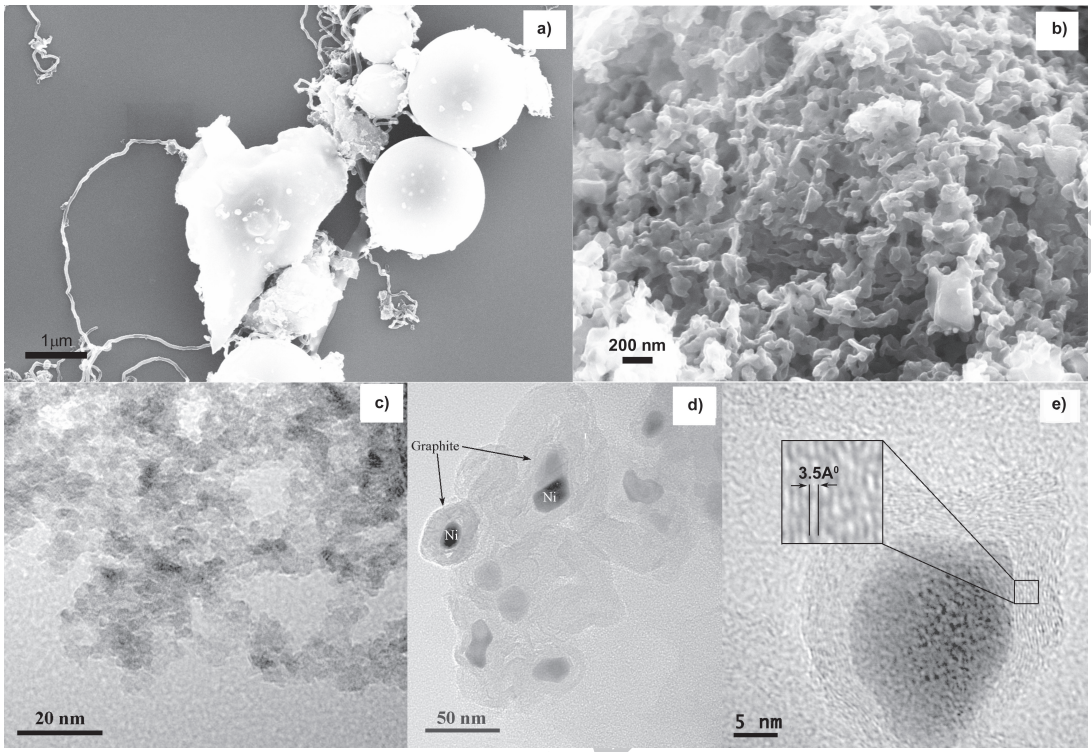

Figure 3: SEM (a, b) and TEM (c, d, e) images of samples S_3, S_2, $S_{0.75}$, S_1 and S_3 respectively.

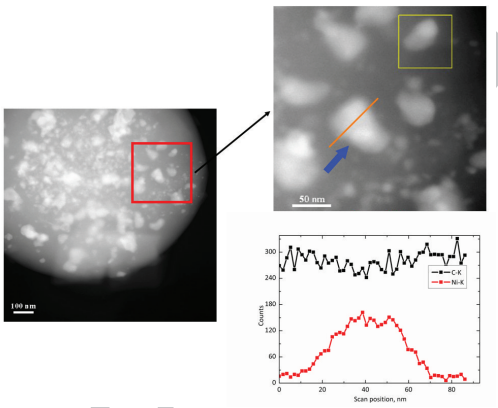

Figure 4: STEM images of sample S_3 and EDX line-scan profile of characteristic X-ray Ni and C lines as a function of electron probe position on the sample.

phologies (see Fig. 3a). It is also possible to synthesize carbon coated Ni nanoparticles in the form of flakes by changing parameters of solid-phase pyrolysis as it has been demonstrated in Fig. 3b. The TEM images in Fig. 3c,d,e show Ni nanoparticles coated by graphite-like shell with 3.5 Å interplanar distance between the graphite layers. The coatings prevent Ni nanoparticles from oxidation and aggregation. Bright regions on carbon sphere STEM images correspond to Ni nanoparticles. The observed distributions of characteristic K-line intensity of nickel and carbon indicates that the Ni particles are indeed ingrained into the carbon spheres. The magnetic moment of a nanoparticle is determined by its average volume, $\langle V \rangle = \frac{\int_0^\infty N(v)dv}{\int_0^\infty N(v)dv}$, where the N(v) is the distribution function of nanoparticles over volumes. For the case of nearly spherical nanoparticles the volume distribution is practicaly equivalent to the linear size distribution, and $\langle d \rangle \approx \sqrt[3]{\langle V \rangle}$. Size distributions of Ni nanoparticles in our samples can be satisfactorily described by a lognormal function, $f(V) = \frac{1}{\sigma V \sqrt{2\pi}} e^{\frac{[-ln(V)-ln(V_0)]^2}{2\sigma^2}}$, where σ is the standard deviation lnV from its average $\ln V_0$ value. Mean values of $< d >$ with their standard deviations are given in Table 1.

3.2. Magnetic measurements

3.2.1. SQUID magnetometry

We have prepared and thoroughly investigated a group of samples with relatively low concentrations of Ni nanoparticles in carbon: c_{Ni} = 0, 0.5, 0.75, 1, 1.5, 2, 2.5 and 3 at.%. The magnetic behaviour of the samples depends not only on c_{Ni}, but also on the nanoparticles size and shape. Our samples are actually crystallite ensembles consisting of superparamagnetic and ferromagnetic single-domain Ni nanoparticles with the particle size in the range of 1–60 nm.

In our previous works [17–19] we have studied in details the paramagnetic and diamagnetic characteristics of carbon matrix ($c_{Ni} = 0$) and have shown that the solid-state pyrolysis of metal-free phthalocyanine H_2Pc yields 3.5 ± 1μm carbon microspheres, consisting of nanographite crystallites and amorphous carbon. We have observed intensive EPR signal with in-

tegral intensity about $5 \cdot 10^{19}$ spin/g. Present magnetic measurements give the concentration of paramagnetic centers of $3 \cdot 10^{19}$ spin/g. We have also measured the diamagnetic susceptibility of $\chi^{Dia} = -1 \cdot 10^{-6} emu \cdot g^{-1} \cdot Oe^{-1}$, which is nearly temperature independent. These data can be interpreted within a framework of carbon magnetism which is currently a subject of intensive research [37, 38]. Both diamagnetic and paramagnetic contributions of a matrix are taken into account in our calculations of magnetization in Ni@C nanocomposites. Main focus of this study is the analysis of ferromagnetic and superparamagnetic properties in nanocomposites Ni@C with Ni concentration: c_{Ni} = 0.5, 0.75, 1, 1.5, 2, 2.5 and 3 at.% (samples $S_{0.5} \div S_3$).

3.2.1.1 Size effects. Interactions of surface Ni atoms with nanographite shell. Giant paramagnetism of ultra-fine nickel particles.

Basic magnetic characteristics are presented in Table 1 and in Figs. 5–17. Magnetic measurements have been performed in a wide range of temperatures (10–300 K) and in external magnetic fields up to 45 kOe. Both structural and magnetic data show that our samples are in fact single-domain ferromagnetic and superparamagnetic ensembles of Ni nanoparticles embedded in a carbon matrix so that their easy axes of magnetization are randomly distributed. It is evident that the ratio between superparamagnetic and ferromagnetic particles primarily depends on c_{Ni}. It is also evident that this ratio changes with temperature and the total magnetization $M^{Tot}(H,T) = M(H,T)$ can be presented as a sum of ferromagnetic, superparamagnetic and diamagnetic contributions:

$$M(H,T) = M^{FM}(H,T) + M_S^{SPM}(T)L(\delta) + \chi^{Dia}H \qquad (3)$$

where $L(\delta) = coth(\delta) - 1/\delta$ is the Langevin function, M_S is saturation magnetization and in last term χ^{Dia} is diamagnetic susceptibility of the carbon matrix.

Fig. 5 shows temperature dependence of the total magnetization for the $S_{0.5} \div S_3$ samples measured in a maximum applied magnetic field of 45 kOe. The curves given on Fig. 5 represent the sum of magnetizations for ferromagnetic and superparamagnetic nanoparticles. Magnetization increase with temperature decrease implies the transition of the "large" particles from superparamagnetic to the blocking ferromagnetic state as well as enhancement of superparamagnetic contribution at low temperatures. The fraction of superparamagnetic particles changes with temperature as $\gamma = 1 - 2M_r/M_S^{FM}$ [39].

Fig. 6 shows the field-dependence magnetization at T = 10-300 K in samples $S_{0.75}$, S_1, S_2 and S_3. Samples clearly demonstrate increase of magnetization in low fields with decreasing temperature. Such behaviour is determined with the transition of nanoparticles from superparamagnetic to the blocking ferromagnetic state. Notice, an abrupt change of magnetization with decreasing temperature in S_3 sample is apparently related to the bimodal size distribution of nanoparticles. The field dependence magnetization at T = 10 and 300K is also presented on Fig. 7 for comparison.

The saturation magnetization for all samples, except $S_{0.5}$ and $S_{0.75}$ was determined by M vs $1/H^2$ plots extrapolated to infinitely large fields. The values of $M^t{}_S^{ot}$ at 10K are presented in Table 1. Linear dependences of M on H in samples of $S_{0.5}$ and $S_{0.75}$ do not allow estimation of M_S values in those samples: they only specify that $M^t{}_S^{ot}$ values in samples are much higher than at H=45kOe.

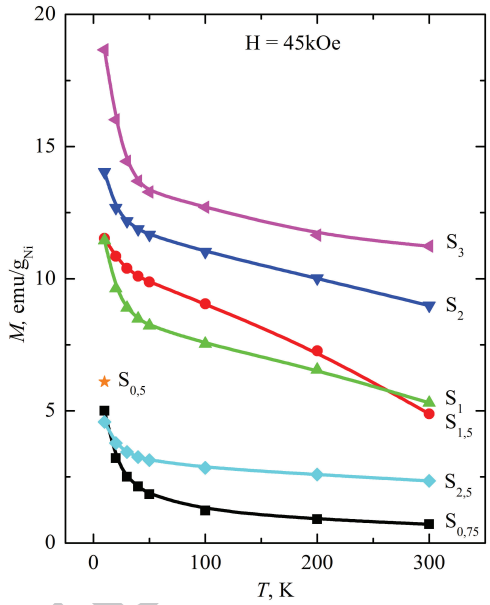

Figure 5: Total magnetization M versus temperature for samples $S_{0.5}$–S_3 at H= 45 kOe.

The most peculiar feature of Ni@C composites magnetic behavior is the abrupt drop in magnetization with decrease in size of Ni nanoparticles (see Figs. 5, 7 and 8, 9). Usually, reduction of nanoparticles magnetization compared to that of bulk can occur for a variety of reasons. Often it is caused by oxidation which results in reduction of a core or otherwise it is caused by existence of thin layers of crystallites with the noncollinear magnetic moments on the surface [31–34]. Other possible explanations involve existence of thin surface paramagnetic ("dead") layers or presence of very small superparamagnetic particles [32]. Formation of the Ni-C metastable solid solution could produce the same effect [27, 35]. However, our samples were prepared at 700°C, where Ni is completely insoluble in graphite, and carbon solubility in nickel is insignificant (about 0.4 at.%). Here magnetization drop in Ni@C composites is believed to result from interaction between Ni nanoparticles and the graphite matrix. A significant suppression of Ni local magnetic moment in Ni@C is obviously due to transfers of electrons from a carbon matrix to nickel. Transfer of electrons on the one hand leads to formation of the "dead " layer consisting of diamagnetic nickel ions according to reaction: $Ni(3d^9 4s^1) + e^- \rightarrow Ni^{1-}(3d^{10}4s^1), \left[FM(Ni) \rightarrow Dia(Ni^{1-})\right)$. On the other hand, considering zone model the electron transfer on nickel leads to reduction of the density of states at the Fermi level. The electron work functions are 4.9 eV in Ni and 4.6 eV in graphite. A smaller work function implies a higher Fermi level and electrons flow from this material to the one with the

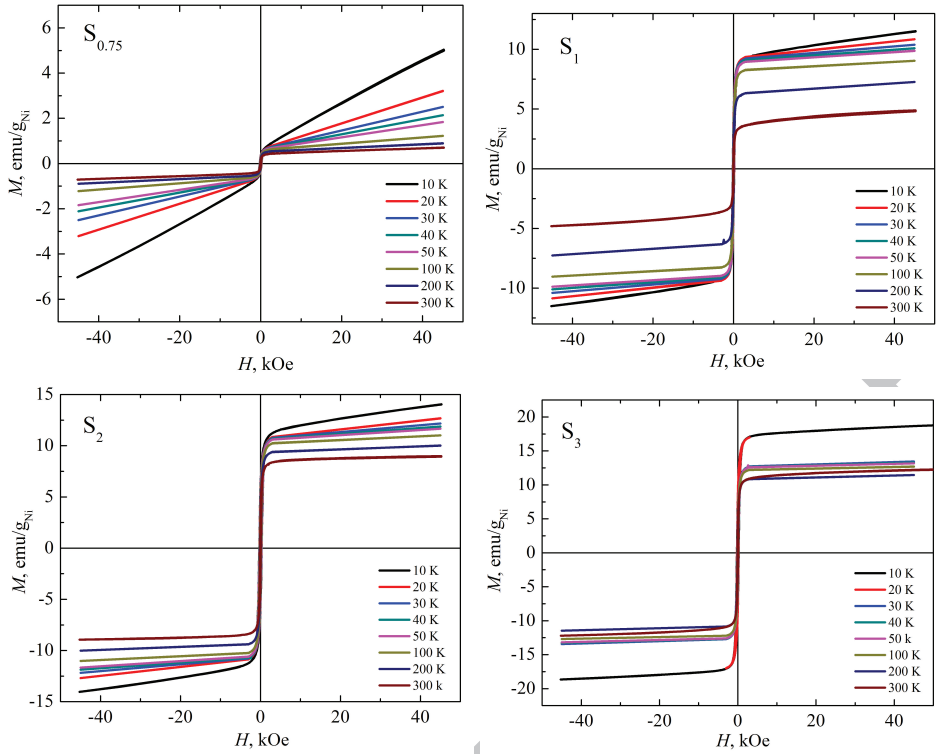

Figure 6: Field-dependence of the magnetization for $S_{0.75}$, S_1, S_2 and S_3 samples at T = 10–300 K

higher work function (lower Fermi energy level). The interaction between a carbon matrix with Ni nanoparticles sharply affects also in EPR spectra. First of all it shows up in rapid falling of integrated intensity and partial broadening of a narrow EPR signal of a carbon matrix at increasing Ni concentration in the samples (see Fig.16). Similarly, in Refs. [40, 41] the magnetization in Ni thin films was described to be very sensitive to a degree of coupling between the Ni d-band and substrate conduction band.

Fig.8 shows dependence of saturation magnetization M_S(Ni@C) (normalized to bulk value M_S(Ni-bulk)) at $T = 10$ K on particle surface-to-volume ratio S/V. If in massive samples the magnetization of Ni is equal $0.6\mu_B$/atom, magnetization in nanocomposites Ni@C at $< d > = 12$ nm is less than one order of magnitude. Linear dependence M_S(Ni@C)/M_S(Ni_{bulk}) vs. S/V has a sharp drop at $< d > \sim 10$ nm. Further down to 4 nm the normalized magnetization of Ni@C nanocompos-ites does not change, while the S/V increases with decreasing $< d >$. This behaviour can be explained in the framework of the "particle in the box" model, according to which the free valence electrons are confined in the "potential well"and are unable to escape the metal. The smaller the particle size is the higher the energy of individual electron states and the larger the distances between energy levels are [42]. The rise of the Fermi levels of Ni nanoparticles upon their size decrease compensates the drop of magnetization arising from the S/V change.

On the other hand a thorough analysis of magnetization curves for samples $S_{0.5}$ and $S_{0.75}$ in Fig.7 (straight lines in the magnetic fields to 45 kOe) specify that at M_S saturation magnetization in these samples can reach considerable values $\sim 10 emu/g_{Ni}$. That giant paramagnetism observed in samples $S_{0.5}$ and $S_{0.75}$ with small sizes is assumed to correspond to large orbital moments of conductive electrons in the ballistic mode. Fig.9 shows size dependence of Ni@C nanocomposites magnetization at $T = 10$ and 300K in magnetic field of 45 kOe. The drop of magnetization is practically zero in the samples $S_{0.5}$ and $S_{0.75}$ at the room temperature. It can be explained by decrease in thermal free path of electrons: $L_T = h\nu_F/\pi k_B T$ (h is Plancks constant, ν_F is the electron Fermi velocity) and by paramagnetic dependence on temperature. Unusual (exotic) ferromagnetism and/or giant paramagnetism in fine nanoparticles particularly in diamagnetic bulk-materials are currently under intensive investigation [29, 43, 44].

Fig.10 shows hysteresis loops for all samples $S_{0.5}$ - S_3 at 10 and 300K. The remanence squareness values $M_{rem}/M^{F}_{sat}{}^{M}$ of Ni@C at $T = 10$ K are given in Table 1. These values are close to the value 0.5 calculated in the framework of Stoner-Wohlfarth model for the ensemble of non-interacting single-domain nanoparticles with uniaxial anisotropy [45]. Stoner-Wohlfarth model gives a value of $M_r/M_s = 0.86$ for nanoparticles with fcc structure and four-fold magnetic anisotropy, which is the case for Ni. However, according to this model, in case of Ni nanoparticles with fcc-structure and four-fold magnetic symmetry (four easy axis) we should expect to have a single domain state with the ratio of $M_r/M_s = 0.86$ (restricted cubic magnetic anisotropy). It is evident that, for Ni/C nanocomposites, one

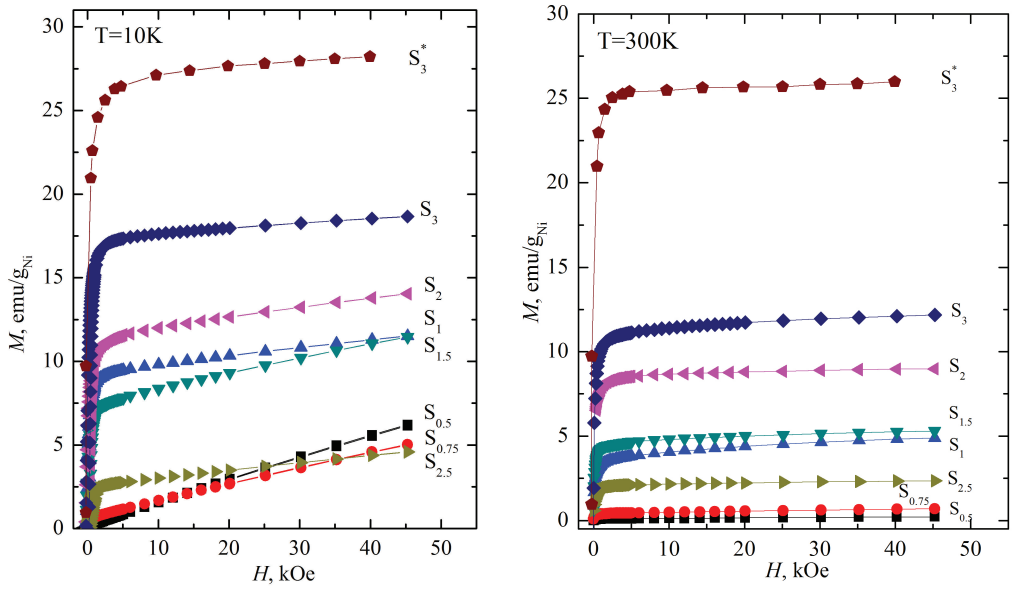

Figure 7: M versus H for samples $S_{0.5}$–S_3^* at T=10 and 300 K.

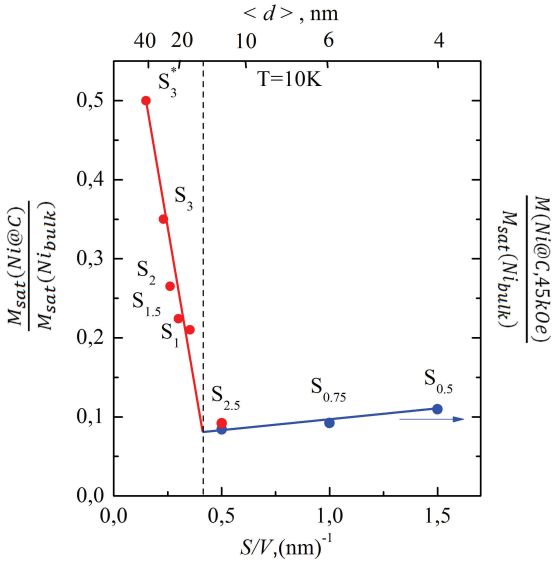

Figure 8: Size dependence of the normalized magnetization of nanocomposites Ni@C at T = 10K.

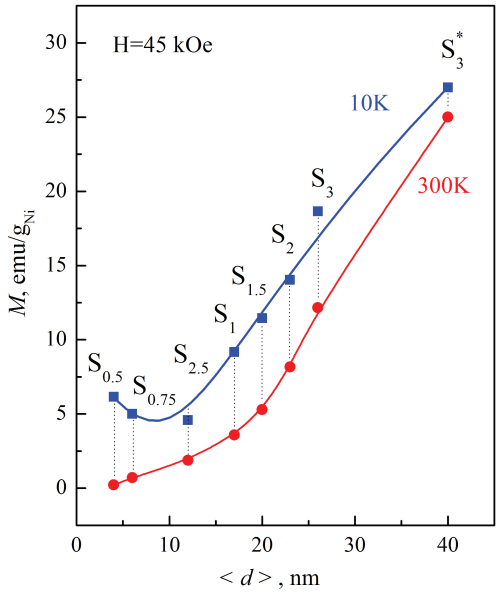

Figure 9: Size dependence of the magnetization of nanocomposites Ni@C at T = 10 and 300K in magnetic field H=45 kOe

should take into account contribution to the uniaxial anisotropy caused by the nonspherical shape of nanoparticles (elongated particles) and crystalline anisotropy. In Refs. [46, 47] a combined Stoner-Wohlfarth model has been developed where the total energy of magnetic anisotropy of a single-domain particle consists of cubic and uniaxial components. Dependence of the remnant magnetization on uniaxial component and its contribution to the total anisotropy has been studied. When the contribution of the uniaxial anisotropy is in the range of 60 - 100 %, the value of M_{rem}/M_{sat} does not practically differ from val-

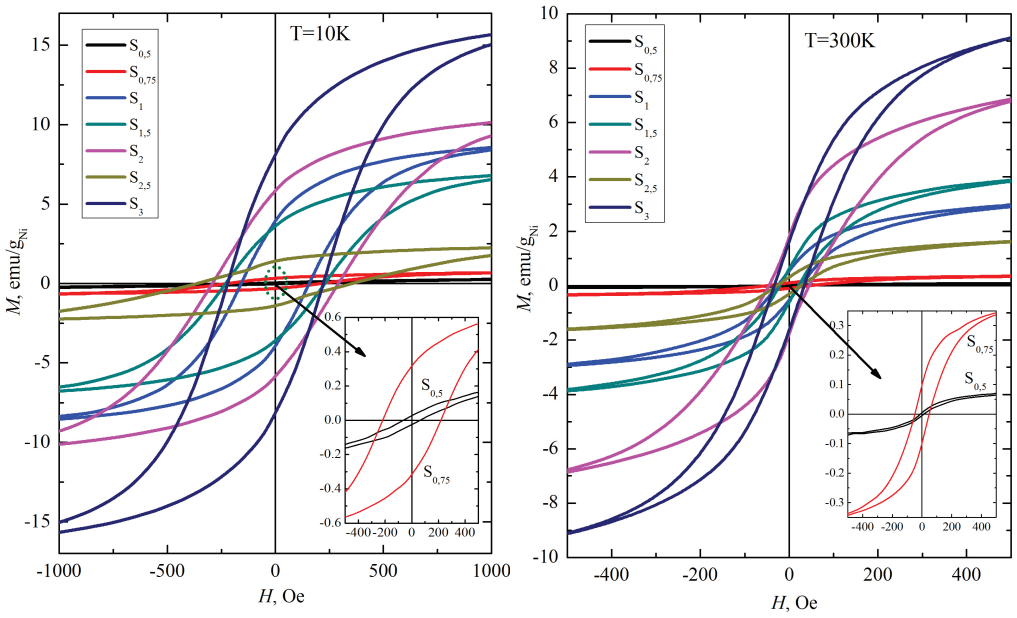

Figure 10: Hysteresis loops for $S_{0.5}$ - S_3 samples at 10 and 300K.

ues characteristic for the models considering only an uniaxial magnetic anisotropy, i.e. $M_{rem}/M_{sat} = 0.5$ [45].

3.2.1.2 Size, temperature and concentration dependencies of coercivity in Ni@C nanocomposites. Surface magnetic anisotropy. High blocking temperatures in fine Ni@C nanocomposites.

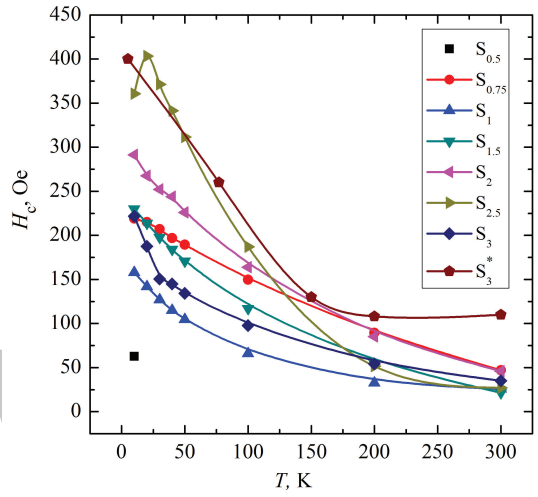

Figure 11: Temperature dependence of coercivity in Ni@C nanocomposites for samples $S_{0.5}$ – S_3.

Figs.11 and 12 show temperature and size dependencies of coercive field H_c in Ni@C nanocomposites (samples $S_{0.5} \div S_3$). The high values of H_c in small size cases such as $S_{0.75}$ and $S_{2.5}$ samples are apparently defined by surface a nisotropy. The influence of surface anisotropy on the hysteresis in fine magnetic particles has been investigated in a number of theoretical and experimental works [48–51]. The coercive force of one-domain magnetic nanoparticles primarily depends on an effective constant of magnetic anisotropy K_{eff} defined by a contribution of two components: volume magnetic anisotropy K_{vol} and surface magnetic anisotropy K_s: [48]

$$K_{eff} = K_{Vol} + 6K_S/d, \tag{4}$$

where d is a nanoparticle diameter. It should be noted that volume anisotropy constant is defined by the magnetocrystalline anisotropy K_a and shape anisotropy K_{sh}, respectively. The magnetocrystalline anisotropy contribution to the coercive field for the ensemble of randomly oriented single-domain nanoparticles can be written as: [2, 52, 53]

$$H_c = \frac{2K_a(T)V_0N}{M_S T}\left[1 - 5\left(\frac{k_B T}{K_a V_0}\right)^{\frac{1}{2}}\right] \tag{5}$$

where V_0 average nanoparticle volume, k_B Boltzmann constant, N number of particles with average volume V_0 with total mass of 1 g. This equation is applicable in the range of temperatures from $T = 0$ to the blocking temperature $T_b = K_a V_0/25k_B$. At $T > T_b$, nanoparticle undergoes a transition into a superparamagnetic state and coercive force vanishes [2, 53]. At $T = 0$, equation (5) reduces to $H_c = 2k_a/M_S$ which becomes the coercive field given by Stoner-Wohlfarth model for spherical single-domain nanoparticle with coherent rotation of magnetization. Decrease of coercive field with increasing temperature is due to both Neel-Brown relaxation [54, 55] and strong temperature dependence K_a(T) of nickel [56].

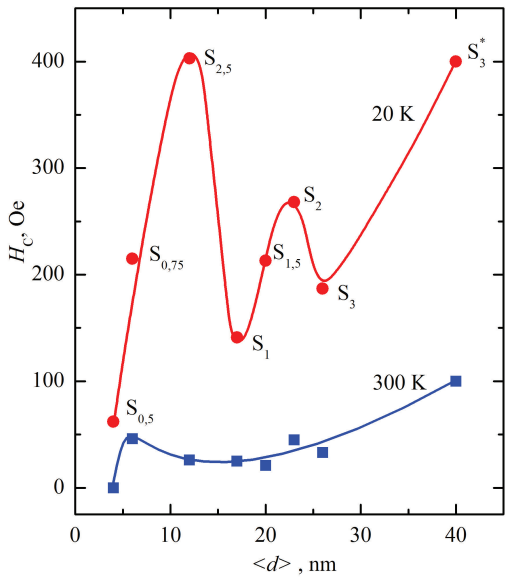

Figure 12: Size dependence of coercivity in Ni@C nanocomposites for samles $S_{0.5} - S_3$ at 20 and 300K.

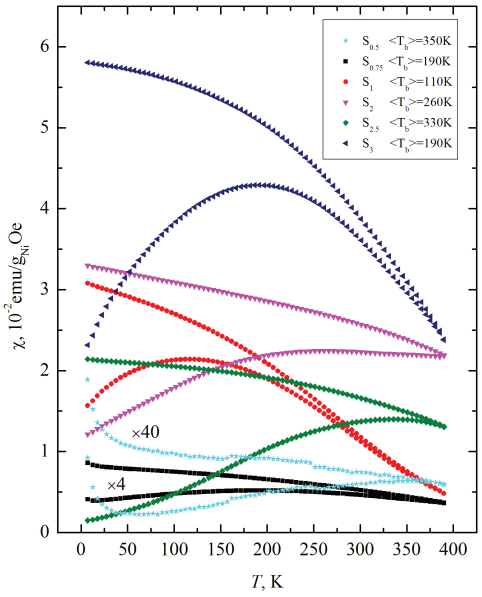

Figure 13: ZFC/FC susceptibility curves of $S_{0.5} \div S_3$ samples under applied fields of 200 Oe.

Shape anisotropy contribution to the coercive field is given as $N_{eff} \cdot M_S$, where N_{eff} is a demagnetizing factor [2, 57].

The values of K_{eff} can be defined by analyzing FC/ZFC curves as it has been shown in Refs. [58–60]. Fig. 13 presents susceptibility temperature dependencies in samples $S_{0.5} \div S_3$ obtained in rather small field in ZFC and FC regimes. The samples have been measured in the field of 200 Oe. All FC/ZFC curves in Fig. 13 are quite broad evidently due to broad particle size distributions. Therefore, we deal with a broad distributions of blocking temperatures with average values of $< T_b >$. The most interesting feature of the curves shown in Fig. 13 is the low values of susceptibility at low temperatures in samples $S_{0.5}$, $S_{0.75}$, $S_{2.5}$. The values of susceptibilities in these sam-ples are smaller by 1 to 2 orders of magnitude (at $T \to 0$), than the ones in S_1, $S_{1.5}$, S_2 and S_3. The dependences of FC/ZFC susceptibility and an effective constant of anisotropy K_{eff} on the average nanoparticle diameter $< d >$ are presented in Fig. 14. The value of K_{eff} is calculated according to a formula $K_{eff} = M_S^2(T)/3\chi^b_{ZFC}$ [22]. The blocking temperature T_b is defined by particle volume and anisotropy effective con-stant $T_b = K_{eff} V_0/25k_B$. In samples $S_{0.5}$, S_1, $S_{1.5}$, $S_{2.5}$ and S_3, average blocking temperatures $< T_b >$ are equal to 350, 110, 200, 330 and 190 K, respectively. High values of $< T_b > =$ (330-350)K for samples $S_{0.5}$ and $S_{2.5}$ with small nanopar-ticle sizes can be apparently explained by substantial energy contribution of surface anisotropy into an effective anisotropy constant, K_{eff}. The fine magnetic nanoparticles with blocking temperatures around 43°C may have important practical appli-cations in medicine for treatment of cancer by adjustable mag-netic hyperthermia method [61].

The fine Ni nanoparticles with blocking temperatures above room temperature are also important for high-density magnetic recording storage. In ensembles of magnetic nanoparticles with high particle density dipole-dipole interactions between nanoparticles have to be taken into account. Such interactions can raise the energy barrier that separates the two energy states of single-domain nanoparticle. Such increase of the energy barrier in turn increases blocking temperature: $T_b \sim (K_a V_0 + E_{dip})/25k_B$

3.2.2. Ferromagnetic and electron paramagnetic resonances in Ni@C nanocomposites. The similarities of concentration dependencies effective g-factor, linewidth of FMR spectra - ΔH_{pp} and coercive field- H_c.

Fig. 15 shows FMR and EPR spectra of the Ni@C nanocomposites (S_0-S_3) with various Ni concentrations (0-3 at.%). The narrow signal at g=2 stems from EPR of carbon matrix and it must be relevant to coupled π - electrons in nanographite crystallites formed inside a carbon microspheres [17, 18]. Wide FMR lines are due to the d-electrons of Ni. As mentioned above, sample S_0 with c_{Ni}=0 has an intensive EPR signal ($\sim 5 \cdot 10^{19}$spin/g) with very narrow line (around 1 Oe). However, even small increase in Ni concentration leads to a drastic drop in integral intensity of the EPR signal. When Ni load reaches 1.5 at.%, the intensity of EPR signal practically drops to zero, while the linewidth increases up to 3.5 Oe (see Fig. 16). Earlier we discussed the magnetization drop in Ni@C composites with decreasing average particle size (see Fig. 8, 9) and that size effect was interpreted as a result of interaction of Ni nanoparticles with carbon matrix, namely electron transitions from graphite-like carbon shell to Ni nanoparticles. The same transitions can obviously decrease the number of unpaired π-electrons and lead to disappearance of the narrow EPR line with c_{Ni} = 1.5-2 at.%. Fig. 17 shows concentration dependences of the g-factor and

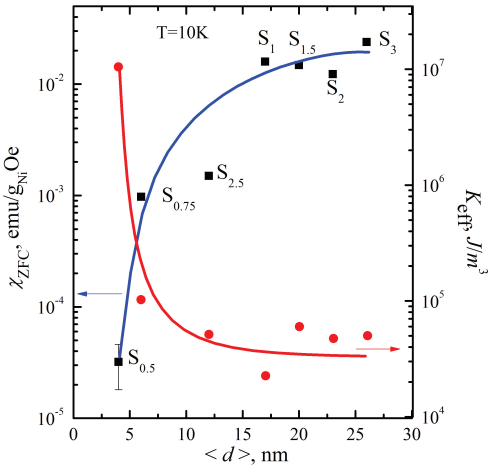

Figure 14: Dependences of low-field ZFC susceptibility and effective constant of anisotropy on the sizes of nanoparticles at T=10K.

FMR linewidth. As it is known, the g-factor of bulk Ni is 2.22 ± 0.02 [62]. The deviation from the bulk value can be explained by the influence of the effective magnetic field B_{eff} witch can be expressed for one domain particle as [63, 64]

$$B_{eff} = B_{app} + B_d + B_a, \quad (6)$$

where B_{app} is the external magnetic field, B_d is the demagnetization field, B_a is the magnetocrystalline anisotropy field. Magnetocrystalline anisotropy field B_a and demagnetization field B_d not only define the value of g-factor, [62–64] but also largely determine the FMR linewidth [36, 65, 66].

For nearly spherical nanoparticles without shape anisotropy the FMR linewidth ΔH is defined as $\Delta H = 4K_a/\pi I_0$, where I_0 is the saturation magnetization per 1 cm^3 [66]. It is clear from Figs. 15 and 17 it is visible that rather small Ni nanoparticles (samples of $S_{2.5}$ and $S_{0.75}$) lead to the noticeable shift of the resonant field (respective to an effective g-factor - g_{eff} growth) and broadening of the absorption FMR line. We believe that the noticeable shift and broadening of FMR signal is defined by its contribution to surface anisotropy.

In Refs. [67, 68] the influence of various types of surface anisotropy (Neel-Brown and Aaroni) on FMR spectra have been investigated for particles from uniaxial volume (K_V) along with uniaxial surface (K_S) anisotropies. For fine nanoparticles, magnetic field of surface anisotropy ($\sim K_S/M_R$) significantly surpasses magnetic field of volume anisotropy ($\sim K_V/M$) which is 106 Oe for Ni at 293K [69]. The widest FMR line ΔH_{FMR} is observed in sample $S_{2.5}$: ΔH_{FMR} (c = 2.5) = 1100 Oe. The FMR signal in sample $S_{2.5}$ is wider by 300-400 Oe than those of with c = 2 and 3. Such broadening is obviously caused by the field of surface anisotropy $\sim K_S/M_R$ and perhaps some contribution to the line width is provided by magnetic dipole - dipole interactions. It is interesting to note the similarities between concentrations dependencies of g_{eff}, ΔH_{FMR} and coercive field H_c

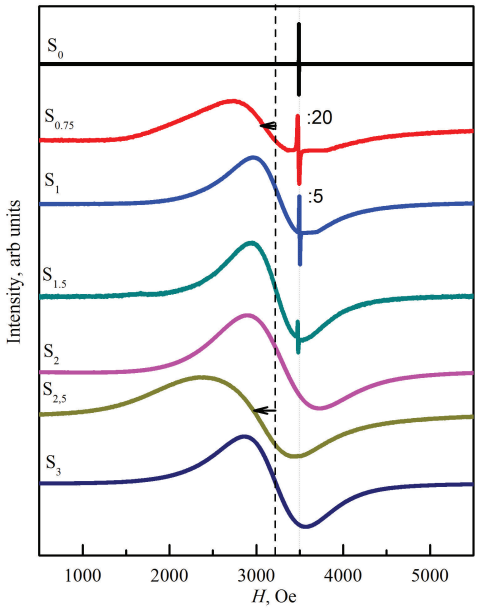

Figure 15: FMR and EPR spectra for samples $S_{0.5}$ – S_3 at X-band and T = 300K.

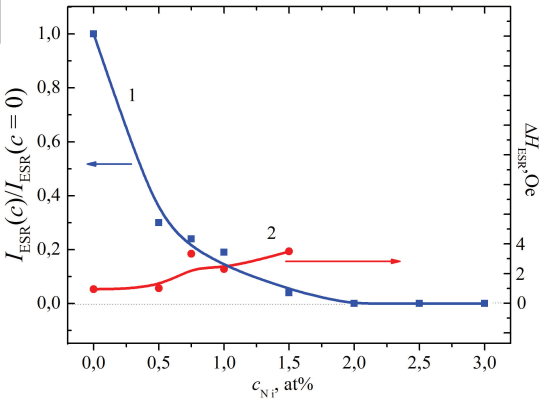

Figure 16: Integrated intensity (1) and linewidth (2) of EPR spectra versus Ni concentration in nanocomposites Ni@C.

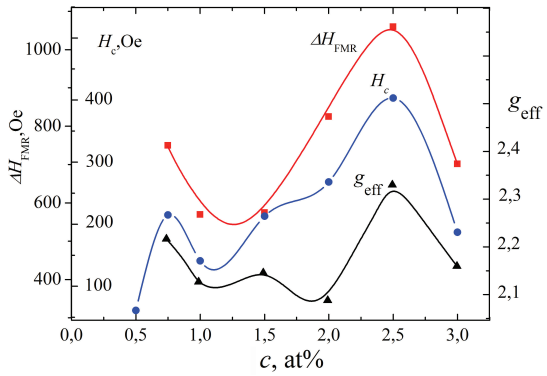

Figure 17: FMR linewidth, effective g-factor and coersivity versus Ni concentration in nanocomposites Ni@C.

which are given in Fig. 17. It is not surprising that all these parameters (g_{eff}, ΔH_{FMR} and H_c) depend on magnetocrystalline anisotropy, shape anisotropy and surface magnetic anisotropy.

Conclusions

Carbon-coated single-domain Ni nanoparticles, Ni@C nanocomposites, have been synthesized using solid-state pyrolysis of nickel phthalocyanine metal-free phthalocyanine $(NiPc)_x(H_2Pc)_{1-x}$, solid solutions where $0 \leq x \leq 1$. Dilution of nickel phthalocyanine with metal-free phthalocyanine and variation of pyrolysis parameters provide unique opportunity for preparation of Ni-C nanocomposites with different Ni concentrations. They have been continuously varied from 0 to 3 at.% (0-12 wt.%) and average single-domain nanoparticles sizes have been obtained from 4 nm to 40 nm. X-ray diffraction data, Raman spectra, SEM and TEM images clearly demonstrate that Ni nanoparticles have fcc structure and are uniformly distributed within the carbon matrix. We have observed both ferromagnetic and superparamagnetic nanoparticles in samples $S_{0.75}$ - S_3 due to the wide size distribution of Ni nanoparticles.

The effects of size and nickel concentration on magnetic characteristics of Ni@C nanocomposites have been investigated. Magnetic measurements show an abrupt drop in magnetization with decrease in size of Ni nanoparticles in the interval of 40 - 12 nm. Magnetization of Ni@C nanocomposites with $< d > \approx 10$ nm is equal to $0.06\mu_B/atom$ at $T = 10$K. It is an order of magnitude less than of bulk samples. Magnetization exhibits almost linear dependence on surface-to-volume ratio, $1/d$. Electron transfer from a carbon matrix to nickel particles leads to the formation of diamagnetic (shell) surface and a reduction in density of states at the Fermi level. Additionally, a noticeable increase in magnetization within the range of 4 nm to 10 nm has been found as a result of the giant paramagnetism determined by the large orbital motion of conductive electrons in the ballistic mode.

In the range of fine Ni nanoparticles (1-10 nm), the contribution of surface magnetic anisotropy leads to increase in effective constant of magnetic anisotropy K_{eff} and accordingly to enhancement of the coercive field. As a result the blocking temperature increases as well.

Finally, effective g-factor g_{eff}, linewidth ΔH_{FMR} from FMR and coercive field H_c from SQUID measurements have been found to have similar dependences on Ni nanoparticle concentration.

Acknowledgements

This work has been supported by the grants of Volkswagen Stiftung project NoA108857 and RA MES State Committee of Science, in the frames of the research project No15T-1C249.

References

[1] S. P. Gubin, Magnetic Nanoparticles, Wiley, Weinheim, 2009.
[2] A. A. Guimaraes, Principles of Nanomagnetism, Berlin, Heidelberg, 2009.
[3] R. Skomski, Nanomagnetics, J. Phys: Condens. Matter 15, (2013) 841-96.
[4] E. Roduner, Nanoscopic Materials: Size-Dependent Phenomena, J. Am. Chem. Soc. 2006.
[5] Q. A. Pankhurst, N. T. K. Thank, S. K. Jones and J. Dobson, Progress in applications of magnetic nanoparticles in biomedicine, J. Phys. D: Appl. Phys. 42 (2009) 224001-14.
[6] L. Zhentao, H. Chao, Y. Chang and Q. Jieshan, Synthesis and characterization of carbon encapsulated magnetic nanoparticles via arc-plasma assisted CVD, J. Nanosci. Nanotechnol, 9 (2009) 7473-76.
[7] E. M. M. Ibrahim, S. Hampel, R. Kamsanipally, J. Thomas, K. Erdmann, S. Fuessel, C. Taeschner, V. O. Khavrus, T. Gemming, A. Leonhardt and B. Buechner, Highly biocompatible superparamagnetic Ni nanoparticles dispersed in submicron-sized C spheres, Carbon, 63 (2013) 358-66.
[8] H. Huang, Q.Xie, M. Kang and B. Zhang, Labeling transplanted mice islet with polyvinylpyrrolidone coated superparamagnetic iron oxide nanoparticles for in vivo detection by magnetic resonance imaging, Nanotechnology, 20 (2009) 365101-1-9 .
[9] J. K. Park, J. Jung, P. Subramaniam and B. P. Shah, Graphite-coated magnetic nanoparticles as multimodal imaging probes and cooperative therapeutic agents for tumor cells, Small, 7 (2011) 1647-52 .
[10] P. Z. Li, A. Aijaz and Q. Xu, Highly Dispersed SurfactantFree Nickel Nanoparticles and Their Remarkable Catalytic Activity in the Hydrolysis of Ammonia Borane for Hydrogen Generation, Angewandte Chemie, 51 (2012) 6753-56.
[11] L. Y. Bai, F. L. Yuan and Q. Tang, Synthesis of nickel nanoparticles with uniform size via a modified hydrazine reduction route, Materials Letters, 62 (2008) 2267-70.
[12] G. Zhang, X. Zhao and L. Zhao, Preparation of single-crystalline nickel nanoflowers and their potential application in sewage treatment, Materials Letters, 66 (2012) 267-9.
[13] T. Jaumann, E. M. M. Ibrahim, S. Hampel, D. Maier, A. Leonhardt and B. Buechner, The Synthesis of Superparamagnetic Cobalt Nanoparticles Encapsulated in Carbon Through High-pressure CVD, Chemical Vapour Deposition, 19 (2013) 228-34.
[14] A. S. Manukyan, A. A. Mirzakhanyan, G. R. Badalyan, G. H. Shirinyan and E. G. Sharoyan, Preparation and characterization of nickel nanoparticles in different carbon matrices, J. Contemp. Phys.(Armenian Ac.Sci.), 45 (2010) 132-36.
[15] A. S. Manukyan, A. A. Mirzakhanyan, G. R. Badalyan, G. H. Shirinyan, A. G. Fedorenko, N. V. Lianguzov, Yu. I. Yuzyuk, L. A. Bugaev and E. G. Sharoyan, Nickel nanoparticles in carbon structures preparedby solid-phase pyrolysis of nickel-phthalocyanine, J. Nanopart. Res. 14 (2012) 982-1-7.
[16] A. S. Manukyan, A. A. Mirzakhanyan, T. K. Khachatryan, G. R. Badalyan, K. G. Abdulvakhidov, L. A. Bugaev and E. G. Sharoyan, Copper-carbon nanocomposites prepared by solid-phase pyrolysis of copper phthalocyanine, J. Contemp. Phys.(Arenian Ac. Sci.), 47 (2012) 292-5.
[17] A. S. Manukyan, A. A. Mirzakhanyan, T. K. Khachatyran, G. R. Badalyan, G. M. Arzumanyan and E. G. Sharoyan, Investigation of carbon microspheres prepared by solid-phase pyrolysis of metal-free phthalocyanine, J. Contemp. Phys. (Armenian Ac. Sci.), 48 (2013) 43-5.
[18] A.S. Manukyan, A.A. Mirzakhanyan, R.D. Khachaturyan, A.T. Gyulasaryan, A.N. Kocharian, Yu.I. Yuzyuk and E.G. Sharoyan, Structure and magnetic properties of carbon microspheres prepared by solid-phase pyrolysis of organic compounds, J. Contemp. Phys.(Arenian Ac. Sci.), 50 (2015) 195-9.
[19] E. Sharoyan, A. Mirzakhanyan, H. Gyulasaryan, C. Sanchez, A. Kocharian, O. Bernal and A. Manukyan, Ferromagnetism of Nanographite Structures in Carbon Microspheres, IEEE Transactions on Magnetics, 52 (2016) 1-3.
[20] Y. Oumellal, Y. Magnin, A. Martnez de Yuso, J. M. Aguiar Hualde, H. Amara, V. Paul-Boncour, C. Matei Ghimbeu, A. Malouche, C. Bichara, R. Pellenq and C. Zlotea Magnetism as indirect tool for carbon content assessment in nickel nanoparticles, Journal of Applied Physics 122 (2017) 213902-1-8.
[21] N. Vnukova, A. Dudnik, S. Komogortsev, D. Velikanov, I. Nemtsev, M. Volochaev, I. Osipova and G. Churilov, Carbon coated nickel nanoparticles produced in high-frequency arc plasma at ambient pressure, Journal of Magnetism and Magnetic Materials, 440 (2017) 164-166.

[22] E. Kats, I. Willner, Integrated nanoparticle-biomolecule hybrid systems: synthesis, properties, and applications, Angew. Chem. Int. Ed. 43 (2004) 6042-108.

[23] M. H. Teng, S. W. Tsai, W. A. Chiou, Magnetic packing of graphite encapsulated nickel nanoparticles. Journal of Alloys and Compounds, 495 (2010) 488-490.

[24] Z. Liu, C. Lv, X. Tan, One-pot synthesis of Fe, Co and Ni-doped carbon xerogels and their magnetic properties, Journal of Physics and Chemistry of Solids, 74 (2013) 1275-80.

[25] A. Berlie, L. Terry and M. Szablewski, Controlling nickel nanoparticle size in an organic/metal-organic matrix through the use of different solvents, Nanoscale, 5 (2013) 12212-12223.

[26] A. A. El-Gendy, E. M. M. Ibrahim, V. O. Khavrus, Y. Krupskaya, S. Hampel, A. Leonhardt, B. Buechner and R. Klingeler, The synthesis of carbon coated Fe, Co and Ni nanoparticles and an examination of their magnetic properties, Carbon, 47 (2009) 2821-8.

[27] V. A. Tsurin, A. Ye. Yermakov, M. A. Uimin, A. A. Mysik, N. N. Shchegoleva, V. S. Gaviko and V. V. Maikov, Synthesis, structure, and magnetic properties of iron and nickel nanoparticles encapsulated into carbon, Physics of the Solid State, 56 (2014) 287-301.

[28] S. J. Lee, J. Jung, M. A. Kim, Y.-R. Kim and J. K. Park, Synthesis of highly stable graphite-encapsulated metal (Fe, Co, and Ni) nanoparticles, J. Mater. Sci. 47 (2012) 8112-7.

[29] R. Greget, G. L. Nealon, B. Vileno, P. Turek, C. Meny, F.Ott, A. Derory, E. Voirin, E. Rivie‘re, A. Rogalev, F. Wilhelm, L. Joly, W. Knafo, G. Ballon, E. Terazzi, J. Kappler, B. Donnio, JL. Gallanim, Magnetic properties of gold nanoparticles: a room-temperature quantum effect, Chem. Phys. Chem. 13 (2012) 3092-7.

[30] P. G. van Rhee, P. Zijlstra, T. G. A. Verhagen, J. Aarts, M. I. Katsnelson, J. C. Maan, M. Orrit, and P. C. M. Christianen, Giant Magnetic Susceptibility of Gold Nanorods Detected by Magnetic Alignment, Phys. Rev. Leff. 111 (2013) 127202-1-5.

[31] L. Neel, Anisotropie magntique superficielleet surstructures d’orientation, J. Phys. Radium, 15 (1954) 225-39.

[32] J. M. D. Coey, Noncollinear Spin Arrangement in Ultrafine Ferrimagnetic Crystallites, Phys. Rev. Lett. 27 (1971) 1140-42.

[33] A. Kamzin, B. Stahl, R. Gellert, G. Klingelhofer, E. Kankeleit, L. G. Olkhovik and D. Vcherashnii, Influence of surface on the effective magnetic fields in alpha-Fe_2O_3 and $FeBO_3$, Physics of the Solid State, 42 (2000) 1691-5.

[34] G. C. Papaefthymiou, Nanoparticle magnetism, Nano Today, 4 (2009) 438-47.

[35] M. Diarra, A. Zappelli, H. Amara, F. Ducastelle and C. Bichara, Importance of Carbon Solubility and Wetting Properties of Nickel Nanoparticles for Single Wall Nanotube Growth, Phys. Rev. Lett. 109 (2012) 185501-1-5.

[36] Yu.I. Petrov, Physics of small particles, Moscow, Nauka, 1982.

[37] T.L. Makarova and F.Palacio, Carbon based magnetism, Elsevier, Amsterdam, 2006.

[38] O.V. Yaziev, of magnetism in graphene materials and nanostructures, Rep. Progr. Phys. 73 (2010) 056501-1-16.

[39] L. Weil, Structure of catalysts and ferromagnetic properties at very low temperatures, J. Chim.Phys. 51 (1954) 715-17.

[40] J. Tersoff and L. M. Falicov, Interface magnetization: Cu films on Ni(100), Phys. Rev. B. 25 (1982) 2959-61.

[41] J. Tersoff and L. M. Falicov, Presence and absence of magnetism in thin Ni films, Phys. Rev. B. 26 (1982) 459-61.

[42] R. W. Kelsall, I. W. Hamley, M. Geoghegan, Nanoscale Science and Technology, Wiley & Sons Ltd, England, 2005.

[43] A. Hernando, P. Crespo, M. A. Garca, M. Coey, A. Ayuela, and P. M. Echenique, Revisiting magnetism of capped Au and ZnO nanoparticles: Surface band structure and atomic orbital with giant magnetic moment, Phys. Status Solidi B. 248 (2011) 2352-60.

[44] S. Trudel, Unexpected magnetism in gold nanostructures: making gold even more attractive, Gold. Bull. 44 (2011) 3-13.

[45] E. C. Stoner and E. P. Wohlfarth, A mechanism of magnetic hysteresis in heterogeneous alloys, Phil. Trans. Roy. Soc. 240 (1948) 599-642.

[46] S. I. Smirnov and S. V. Komogortsev, Magnetization curves of randomly oriented ferromagnetic single-domain nanoparticles with combined symmetry of magnetic anisotropy, J. Magn. Magn. Mater. 320 (2008) 1123-7.

[47] S. V. Komogortsev, S. I. Smirnov, N. A. Momot and R. S. Iskhakov, Technique for Determination the Energy of Uniaxial and Cubic Magnetic Anisotropy in Magnetic Nanoparticles from Experimental Magnetization Curve, Journal of Siberian Federal University: Mathematics & Physics, 3 (2010) 515-20.

[48] F. Bodker, S. Morup and S. Linderoth, Surface effects in metallic iron nanoparticles, Phys. Rev. Lett. 72 (1994) 282-85.

[49] D. A. Dimitrov and G. M. Wysin, Effects of surface anisotropy on hysteresis in fine magnetic particles, Phys. Rev. B. 50 (1994) 3077-84.

[50] D. A. Dimitrov and G. M. Wysin, Magnetic properties of spherical fcc clusters with radial surface anisotropy, Phys. Rev. B, 51 (1995) 11947-50.

[51] M. Respaud, J. M. Broto, H. Rakoto, A. R. Fert, L. Thomas, B. Barbara, M. Verelst, E. Snoeck, P. Lecante, A. Mosset, J. Osuna, T. O. Ely, C. Amienis and B. Chaudret, Surface effects on the magnetic properties of ultrafine cobalt particles, Phys. Rev. B. 57 (1998) 2925-35.

[52] C. P. Bean and J. D. Livingston, Superparamagnetism, J. Appl. Phys. 30 (1959) 120-129.

[53] J. Carrey, B. Mehdaoui and M. Respaud, Simple models for dynamic hysteresis loop calculations of magnetic single-domain nanoparticles: Application to magnetic hyperthermia optimization, J. Appl. Phys. 109 (2011) 083921-1-17.

[54] L.Neel. C.R. Hebd, Influence of thermal fluctuations on the magnetization of ferromagnetic small particles, Seances Acad. Sci. 5 (1949) 99-136.

[55] W. F. Brown, Thermal Fluctuations of a Single-Domain Particle, Jr. Phys. Rev. B. 130 (1963) 1677-86.

[56] R. M. Bozorth, Ferromagnetism, IEEE Press, New York, 1993.

[57] S. P. Gubin, Yu. A. Koksharov, G. B. Khomutov and G. Yu. Yurkov, Magnetic nanoparticles: preparation, structure and properties, Russian Chemical Reviews, 74 (2005) 489-520.

[58] C. Antoniak, J. Lindner and M. Farle, Magnetic anisotropy and its temperature dependence in iron-rich Fe_xPt_{1-x} nanoparticles, Europhys. Lett. 70 (2005) 250-6.

[59] C. Antoniak, J. Lindner, V. Salgueirino-Maceira and M. Farle, Multifrequency magnetic resonance and blocking behavior of Fe_xPt_{1-x} nanoparticles, Phys. Status Solidi, A 203 (2006) 2968-73.

[60] O. Margeat, M. Tran, M. Spasova and M. Farle, Magnetism and structure of chemically disordered $FePt_3$nanocubes, Phys. Rev. B. 75 (2007) 134410-1-7.

[61] F. Pineux, R. Marega, A. Stopin, A. La Torre, Y. Garcia, E. Devlin, C. Michiels, A. Khlobystov and D. Bonifazi, Biotechnological promises of Fe-filled CNTs for cell shepherding and magnetic fluid hyperthermia applications, Nanoscale, 7(48 (2015)) 20474-88.

[62] C. Kittel, Introduction to Solid State Physics, Introduction to Solid State Physics, 8nd edn, Wiley, New York, 2005.

[63] R. Berger, J.-C. Bissey and J. Kliava, Line shapes in magnetic resonance spectra, J. Phys.: Condens. Matter. 12 (2000) 9347-60.

[64] R. Berger, J.-C. Bissey, J. Kliava, H. Daubric and C. Estournes, Temperature dependence of superparamagnetic resonance of iron oxide nanoparticles, Magn. Magn. Mater. 234 (2001) 535-44.

[65] J. H. Van Vleck, Concerning the Theory of Ferromagnetic Resonance Absorption, Phys. Rev. 78 (1950) 226-74.

[66] Y.G. Dorfman, On the Theory of the Influence of Ferromagnetic Particles on EPR Spectra of Dielectrics, JETP. 21 (1965) 472-4.

[67] V.P. Shilov, J. C. Bacri, F. Gazeau, F. Gendron, R. Perzynski and Yu. L. Raikher, Effect of unidirectional anisotropy on the ferromagnetic resonance in ferrite nanoparticles, Phys. Rev. B. 60 (1999) 11902-5.

[68] V. P. Shilov, J. C. Bacri, F. Gazeau, F. Gendron, R. Perzynski and Yu. L. Raikher, J. Appl. Phys. 85 (1999) 6642-7.

[69] V. Singh and M. S. Seehra, Temperature and size dependence of electron magnetic resonance spectra of Ni nanoparticles embedded in an amorphous SiO_2 matrix, J. Phys.: Condens. Matter, 21 (2009) 456001-1 - 9.

Highlights

- Carbon-coated nickel nanoparticles, Ni@C nanocomposites with average sizes of Ni nanoparticles in a range of 4–40 nm were synthesized.
- The size dependence of the magnetic properties of Ni@C nanocomposites were investigated by SQUID magnetometry and magnetic resonance methods.
- The saturation magnetization drops abruptly with decreasing size of Ni nanoparticles in the range 40–12 nm.
- The giant paramagnetism was observed with decreasing the size of Ni nanoparticles within the range of 10–4 nm.
- The similarities between the concentration dependences of FMR parameters such as effective g-factor, FMR linewidth and coercive field H_c were observed.